Changes in dielectric permittivity and shear wave velocity during concentration diffusion

J.C. Santamarina and M. Fam

Abstract: This paper documents a study of concentration diffusion with complementary mechanical and electromagnetic wave measurements. The paper starts with a review of the fundamentals of interparticle forces and wave–geomedia interaction. Experimental data were collected during the diffusion of a high-concentration solution of potassium chloride through different soils with different boundary conditions. Bentonite and kaolinite contracted during diffusion. The interaction between the concentration gradient, true interparticle forces, and fabric changes produced a pore-water pressure front that advanced ahead of the concentration front. The complex permittivity changed with the advance of the concentration front, reflecting the decrease in moisture content and the increase in conductivity. Concentration diffusion affected shear wave propagation through changes in true interparticle forces. Bentonite showed a significant increase in shear wave velocity, whereas the velocity of propagation in kaolinite decreased. Published differences in the behavior of bentonite and kaolinite were compiled and hypotheses are proposed to explain observed phenomena.

Key words: mechanical waves, electromagnetic waves, clays, diffusion, double layer.

Résumé : Cet article documente une étude de la diffusion de concentration au moyen de mesures complémentaires d'ondes mécaniques et électromagnétiques. En premier lieu, une revue des notions fondamentales des forces interparticules et de l'interaction onde–sol est présentée. Des données expérimentales ont été recueillies au cours de la diffusion d'une solution à forte concentration de chlorure de potassium à travers différents sols avec différentes conditions aux frontières. La bentonite et le kaolin se sont contractés durant la diffision. L'interaction entre le gradient de concentation, les forces interparticules réelles et les changements de fabrique ont produit un front de pression interstitielle qui a progressé à l'avant du front de concentration. La permittivité complexe a changé avec l'avancement du front de concentration, réflétant la diminution de teneur en eau et l'accroissement de la conductivité. La diffusion de la concentration a affecté la propagation de l'onde de cisaillement par suite des changements dans les forces interparticules réelles. La bentonite a montré une augmentation significative de la vitesse de l'onde cisaillement, alors que la vitesse de propagation dans le kaolin a diminué. Les différences de comportement disponibles dans la littérature entre la bentonite et le kaolin sont compilées et des hypothèses sont proposées pour expliquer les phénomènes observés.

Mots clés : ondes mécaniques, ondes électromagnétiques, argiles, diffusion, double-couche.

[Traduit par la rédaction]

Introduction

Changes in pore-fluid concentration induce changes in the behavior of fine soils. Concentration decreases, for example, in the case of marine clays flushed with fresh water, e.g., Leda clay. On the other hand, the pore-fluid concentration increases in the case of clay barriers that are used to limit the migration of chemical wastes. Wave-based monitoring techniques can be used nonintrusively to study and to monitor diffusion processes without appreciable disturbance. Furthermore, reflection and transmission wave propagation measurements can be inverted to obtain local values about the global distribution of a parameter using tomographic techniques.

Newtonian-mechanical and Coulombian-electrical forces coparticipate in governing the behavior of geomaterials. Mechanical and electromagnetic waves can probe changes in these forces. For a given material, velocity and attenuation at different frequencies show different features of wave–material interaction revealing inherent material characteristics.

This paper presents an experimental study of concentration diffusion with wave measurements. The aim was to gain better insight into the diffusion process through fine-grained particulate materials, to learn about the effect of true effective stresses on the propagation of shear waves, and to develop the foundations for a site monitoring diffusion

Received August 8, 1994. Accepted February 21, 1995.

J.C. Santamarina and M. Fam. Civil Engineering Department, University of Waterloo, Waterloo, ON N2L 3G1, Canada.

process with wave-based technology. The conceptual framework involves the diffusion phenomenon, the consequent changes in true effective stresses in soil, and the interaction of mechanical and electromagnetic waves with geomedia. These phenomena and concepts are reviewed first, followed by a discussion of experimental procedures and results.

Diffusion: True effective stress

Chemical diffusion

Chemical diffusion is the equalization of differences in concentration within the medium, whereby chemical species move between different concentrations. The diffusion phenomenon results from the brownian movement of elements. The movement of a solvent under a concentration gradient is called chemical osmosis and it is governed by Fick's laws. The mass flux, J, is in direct relation with the concentration gradient according to Fick's first law, whereas, the one-dimensional diffusive transport is modeled by Fick's second law:

$$[1] \quad J = -D_o \frac{\partial c}{\partial z} \qquad \text{Fick's first law}$$

$$[2] \quad \frac{\partial c}{\partial t} = D_o \frac{\partial^2 c}{\partial z^2} \qquad \text{Fick's second law}$$

where c is concentration, z is the direction of flow, t is time, and D_o is the free solution diffusion coefficient. This coefficient D_o is related to the absolute mobility of the diffusing element, which is the maximum velocity that can be attained under a unit chemical potential. The temperature T, the viscosity η of the solution, and the radius a of the diffusing chemical species affect the diffusion coefficient:

$$[3] \quad D_o = \frac{kT}{6\pi\eta a}$$

where k is Boltzmann's constant. This expression can be derived either from the analysis of brownian movement or from thermodynamic principles (Everett 1988). Different correction factors were proposed to account for deviations in diffusion phenomena in soils, including porosity <1.0, tortuosity along weaving intergranular paths, dispersion, and sorption (Rowe et al. 1988; Shachelford and Daniel 1991).

Clay particles with their balancing cations behave as semipermeable membranes. "Ideal" semipermeable membranes prevent passage of certain components in the solution. However, clays are "leaky" semipermeable membranes: they can not completely prevent passage of components, but they can restrict their movement. The "osmotic efficiency" is a measure of "leakiness" and characterizes the efficiency of a clay to undergo hydraulic flow under an osmotic pressure gradient (Mitchell 1991). An osmotic efficiency of 1.0 indicates an ideal membrane, however, a zero value indicates no membrane properties. Knowing the exiting and entering concentrations, the osmotic efficiency can be calculated. Fritz and Marine (1983) concluded that maximum osmotically induced hydraulic pressure can be encountered when a low porosity clay membrane having high cation exchange capacity separates dilute solutions.

True effective stress

The concept of true effective stress was introduced by Bolt (1956) and was adopted by many researchers to explain changes in clay properties with changes in pore-fluid chemistry (Sridharan and Sivapullaiah 1987). Mathematically, the true effective stress, σ_m is

$$[4] \quad \sigma_m = \sigma_{tot} - u_o - (Rep - Att)$$

where σ_{tot} is the total stress, u_o is the pore-fluid pressure, *Rep* is the interparticle repulsion, and *Att* is the interparticle attraction. Stresses *Rep* and *Att* are electrical in nature and manifest through multiple short-range and long-range phenomena (e.g., Morgenstern 1969). Their importance increases in fine-grained materials with high specific surface. Accordingly, the difference between the intergranular pressure and the conventional mechanical effective stress is the interparticle attractive minus repulsive stresses. If the repulsive stress is equal to the attractive stress, or if they are too small compared with the total stress, there will be no difference between the effective stress and the intergranular pressure.

Double layers form in response to electrostatic Coulombian forces between electrically charged particles, ions, and polar–polarized fluid materials. According to Gouy-Chapman's theory (Shang et al. 1994; van Olphen 1977)

$$[5] \quad \vartheta = \sqrt{\frac{\varepsilon_o \kappa' RT}{2F^2 c_o v^2}}$$

where ε_o is the permittivity of a vacuum, κ' is the relative permittivity, R is the universal gas constant, T is temperature in kelvin, F is Faraday's constant, c_o is the bulk concentration, and v is the valence. The parameter ϑ can be used to characterize the "thickness" of the double layer.

Long-range osmotic *repulsion* decreases when the thickness of the double layer around particles decreases. Let's assume that the surface potential ψ_o is high (usual case in clays, where $\psi_o > 25$ mV), yet that particles are sufficiently far apart so that the mid-plane potential is low. Then, the repulsion force between two parallel planar surfaces at distance d can be computed as (Israelachvili 1991)

$$[6] \quad Rep = 64(RTc_o)e^{-d/\vartheta} \qquad \text{(large interparticle distance)}$$

An alternative hypothesis is to assume that the second derivative of the potential with respect to distance is the same between two parallel particles as it is in a single particle. Furthermore, if the effect of anions is disregarded, the following equation for the repulsion pressure can be derived (derivation is similar to that by Yong and Warkentin 1975):

$$[7] \quad Rep = 2(RTc_o)\left(\frac{2\pi^2\vartheta^2}{d^2} - 1\right)$$

(short interparticle distance)

This equation was derived assuming infinite potential at the surfaces of the clay, $\psi_o = \infty$. An increase in d by 2 to

8 Å (1 Å = 0.1 nm) is sufficient to correct for the real surface potential. Both eqs. 6 and 7 disregard the formation of the Stern layer and its shielding effect. Equations 6 and 7 predict similar values for $d \approx 2\vartheta$.

van der Waals – London *attraction* forces arise from the interaction of fluctuating electronic dipoles with the induced dipoles in adjacent atoms or molecules. The van der Waals interaction between two parallel particles suspended in a medium at a distance d is calculated using London's theory:

$$[8] \qquad Att = \frac{A}{6\pi d^3}$$

where the Hamaker constant A can be evaluated from Lifshits' theory using the dielectric permittivity of the interacting media at different frequencies (Israelachvili 1991). Sridharan and Rao (1979) showed an inverse relationship between the Hamaker constant and the static permittivity of the medium; however, Moore and Mitchell (1974) found more complex trends. Lifshitz's theory was used to compute A for different organic fluids between two silica sheets; results presented in Table 1 indicate that the attraction force may vary by a factor of 7. The lowest attraction force occurs when the permittivity of the fluid approaches the permittivity of the soil particle. The value of A is very sensitive to the refractive index assumed for soil particles. The Hamaker constant, A, does not vary for separations less than 15 nm, but it decreases for larger separations (Lyklema 1991). The effect of ionic concentration on van der Waals forces can be predicted from the change in the permittivity with concentration, which is low. However, the screening of charges may reduce the attraction force by 30% (Israelachvili 1991).

When attraction and repulsion forces are considered simultaneously, the following main observations can be made (based on eqs. 6 or 7, and 8). *Observation 1*: the change in concentration and (or) valence affects primarily double layer repulsion: if concentration or valence increases, repulsion decreases, and the effective stress increases. *Observation 2*: the decrease in permittivity produces a decrease in attractive forces that is independent of distance, and a decrease in repulsive forces that is a function of distance (from eq. 6 or 7, the higher the interparticle distance, the greater the loss in repulsion). It can be shown using eqs. 6 and 8 that if the interparticle distance $d > \sim 2$–5 nm, the effective stress will increase when the permittivity changes from 79 to 10. The opposite is true for interparticle distance $d < \sim 2$ nm.

Pore fluid and soil behavior (prior experimental studies)

Changes in clay properties as a result of changing the chemistry of the pore fluid (e.g., permeability, sedimentation rate, Atterberg limits, consolidation, and shear strength) can be analyzed in the light of these observations. Table 2 summarizes experimental results. In general, the trends for changes in concentration and valence are the same both in kaolinite and montmorillonite, as predicted by observation 1. However, trends are opposite when the two clays are subjected to permittivity changes. In this case, observation 2 must be taken into consideration:

Table 1. Calculated Hamaker constant between two silica sheets isolated by different fluids.

Fluid	Static permittivity	Hamaker constant ($\times 10^{-20}$ J)
Carbon tetrachloride	2.3	0.09
Trichloroethylene	3.4	0.10
Chlorobenzene	5.6	0.33
Phenol	9.8	0.48
Benzyl alcohol	13.1	0.48
Acetone	20.7	0.32
Ethanol	24.6	0.33
Methanol	32.6	0.61
Water	78	0.64
Water (high concentration)[a]	78	0.42

[a]Estimated assuming zero static component.

the higher force per particle in kaolinites for a given state of confinement brings particles closer together than in bentonites. Thus, the loss in repulsion prevails in bentonite, while the loss in attraction prevails in kaolinites.

There are other differences. Interparticle arrangements may change if soils are mixed with different fluids prior to fabric formation, e.g., sedimentation test (note differences in test procedures in Table 2). Some clay minerals are known to have a surface charge that is pH dependent. In particular, kaolinite shows positive edge charge when pH approaches 5 (Yong and Warkentin 1975), pH influences double layer repulsion, however, van der Waals attraction is not sensitive to pH. Finally, short-range hydration forces may become involved in kaolinites (further discussed in sequel). These additional effects may clarify some of the unexplained contradictions in Table 2.

It can be concluded, that in most observed cases, the behavior of both bentonites and kaolinites is predictable, at least in qualitative terms, by taking into consideration double layer repulsion, van der Waals attraction, the true effective stress concept, and the related shearing resistance.

Wave–geomedia interaction

Electromagnetic waves and geomedia (concentration)

The dielectric permittivity of a material is a measure of its electrical polarizability due to the application of an electric field. There are several polarization mechanisms, including electronic and ionic resonance, molecular polarization, and spatial Maxwell–Wagner and double layer polarization. Permittivity is a complex parameter; the real component reflects the polarizability of the material, while the imaginary permittivity characterizes Ohmic and polarization losses. The polarization of the material increases from high to low frequencies. The polarization vector that reflects the number of dipole moments per unit volume, can be written as (von Hippel 1954)

$$[9] \qquad \boldsymbol{P} = \varepsilon_o(\kappa' - 1)\boldsymbol{E}$$

where $\boldsymbol{E}$ is the applied external field.

The static relative permittivity of dilute solutions is directly related to the square root of concentration (Debye–

Table 2. Differences between kaolinite and montmorillonite.

Sample preparation	Observed trends: Kaolinite[a]	Observed trends: Montmorillonite[a]	Reference
Hydraulic conductivity			
Hydraulic conductivity was estimated from consolidation tests; air-dried samples were mixed with ethyl alcohol, centrifuged, dried, and then fluids were added	$\kappa' \downarrow \Rightarrow k_p \downarrow$[b]	$\kappa' \downarrow \Rightarrow k_p \uparrow$	Madsen and Mitchell (1989) Mesri and Olsen (1971)
Kaolinite samples were compacted and bentonite samples were consolidated from slurry; hydraulic conductivity was measured using flexible wall permeameter during fluid exchange	$\Delta\kappa' \downarrow \Rightarrow k_p \downarrow$ or remains constant	$\Delta\kappa' \uparrow \Rightarrow k_p \downarrow$	Bowders (1985) (from: Madsen and Mitchell 1989)
Homoionic samples were prepared by repeated washing the clay with 1 N solution of the required ion; the excess solution was removed by distilled water	$c \uparrow \Rightarrow k_p \uparrow$	$c \uparrow \Rightarrow k_p \uparrow$	Mesri and Olsen (1971) Dunn and Mitchell (1984) Quirk and Schofield (1955)
Sedimentation			
Samples were prepared by mixing dry clay with water and carbon tetrachloride, respectively	$\kappa' \uparrow \Rightarrow e \downarrow$	$\kappa' \uparrow \Rightarrow e \uparrow$	University of Waterloo
Samples were mixed with water; salt was added after hydration; after vigorous mixing, they were allowed to settle	$c \uparrow \Rightarrow e \downarrow$ $v \uparrow \Rightarrow e \downarrow$	$c \uparrow \Rightarrow e \downarrow$ $c \uparrow \Rightarrow e \downarrow$	University of Waterloo
Liquid limit			
Samples were mixed with different organic fluids; liquid limit was determined using cone penetrometer test, and reported in terms of volumetric water content to avoid the effect of the variable unit weight of the fluids	$\kappa' \uparrow \Rightarrow LL \downarrow$ Not monotonic	$\kappa' \uparrow \Rightarrow LL \uparrow$	Sivapullaiah, and Sridharan (1987) University of Waterloo
Samples were mixed with aqueous solutions of different valence at different concentrations	$c \uparrow \Rightarrow LL \downarrow$[c] $LL_{Ca} > LL_{Na}$	$c \uparrow \Rightarrow LL \downarrow$ $LL_{Ca} < LL_{Na}$	Mesri and Olsen (1970) Yong and Warkentin (1975) University of Waterloo
Consolidation			
Samples were mixed with different organic fluids and then consolidated	$\kappa' \uparrow \Rightarrow e \downarrow$	$\kappa' \uparrow \Rightarrow e \uparrow$	Sridharan and Sivapullaiah (1987)
Clays were mixed with water, consolidated, and then carbon tetrachloride was added at 12.5 kPa	$\Delta\kappa' \downarrow \Rightarrow e \uparrow$	$\Delta\kappa' \downarrow \Rightarrow e \downarrow$	Sridharan and Rao (1973)
Clays were mixed with carbon tetrachloride, consolidated, and then water was added at 12.5 kPa	$\Delta\kappa' \uparrow \Rightarrow e \downarrow$	$\Delta\kappa' \uparrow \Rightarrow e \uparrow$	Sridharan and Rao (1973)
Samples were prepared using the slurry technique; they were consolidated to 105 kPa in an isotropic cell before adding KCl solution (4.0 M)	$\Delta c \uparrow \Rightarrow e \downarrow$[d]	$\Delta c \uparrow \Rightarrow e \downarrow$	University of Waterloo (this study)
Shear wave velocity			
Samples were prepared using the slurry technique; they were consolidated to 105 kPa in an isotropic cell before adding KCl solution (4.0 M)	$\Delta c \uparrow \Rightarrow V_s \downarrow$	$\Delta c \uparrow \Rightarrow V_s \uparrow$	University of Waterloo (this study)
Shear strength			
Oven dried samples were statically compacted inside the direct shear box, and loaded to the desired stress; samples were flooded with different organic fluids; finally shear was applied	$\kappa' \downarrow \Rightarrow C^* \uparrow$ $\kappa' \downarrow \Rightarrow \phi \uparrow$	$\kappa' \downarrow \Rightarrow C^* \uparrow$ $\kappa' \downarrow \Rightarrow \phi \uparrow$	Sridharan and Rao (1979)
Homoionic samples were prepared as described under hydraulic conductivity (the effect of concentration change decreased for higher confining pressure); shear box or ring shear device were used	Not monotonic	$c \downarrow \Rightarrow C^* \downarrow$ $c \downarrow \Rightarrow \phi \downarrow$	Mesri and Olsen (1970) Kenney (1967) Moore (1991) DiMaio and Fenelli (1994)

Notes: Variables: κ', dielectric permittivity; $\Delta\kappa'$, change in the permittivity of pore fluid; c, concentration; Δc, change in concentration of the pore water; v, cation valence. Parameters: k_p, hydraulic conductivity; LL, liquid limit; e, void ratio; V_s, shear wave velocity; C^*, shear intercept; ϕ, angle of shearing resistance.

[a]The characteristics of kaolinite and bentonite vary among authors. In all cases, kaolinite has low specific surface, whereas, montmorillonite has high specific surface.

[b]Contradictory data were also reported by Madsen and Mitchell (1989).

[c]At pH = 10, the liquid limit increases with concentration (Warkentin 1961)

[d]If permeate is of lower concentration, early collapse may take place followed by swelling (Barbour and Yang 1993).

Table 3. Physical, chemical, and engineering properties of tested soils.

Soil type	Silica flour	Kaolinite	Bentonite
Source	Indusmin Co., Toronto	Vanderbilt Co., Los angeles	Saskatchewan
Trade name	Silex Regular	Peerless clay	Avonseal or Geoseal
Color	White	Light cream	Light tan
Specific gravity, G_s[a]	2.65	2.6	2.55
Liquid limit (%)[a]	na	50	250
Plastic limit (%)[a]	na	35	50
Main cation[b]	—	Sodium	Sodium
CEC (mequiv./100 g)	—	20–30	80–85
pH value[c]	7.8 (10% solids)	4.8 (10% solids)	9.0 (5% solids)
Conductivity (mS/cm)[c]	0.10 (10% solids)	0.04 (10% solids)	1.12 (5% solids)

Notes: Values provided by suppliers unless specified. CEC, cation exchange capacity.
[a]University of Waterloo, standard ASTM procedure.
[b]University of Waterloo, ion chromatography on extracted fluid (bentonite: centrifuge; kaolinite: filtration).
[c]University of Waterloo, solids in suspension.

Huckel theory). For concentrations between 0.1 and 1.0 M the permittivity of water decreases with concentration. This results from the attraction of water molecules around ions, reducing the ability of water to orient with the external field. The imaginary permittivity increases primarily with concentration because of the contribution of the DC losses. Finally, the relaxation time also changes with the increase in concentration: a spread in relaxation times develops and the average relaxation time increases (Hasted 1973).

The complex permittivity of soil mixtures is sensitive to chemical changes in the pore fluid. The permittivity at GHz frequencies reflects the amount of free water and it is governed by the volumetric water content rather than the gravimetric water content (recall that permittivity is the number of dipole moments per unit volume). Soil permittivity increases slowly with volumetric moisture content. After reaching a transition moisture content, not necessarily well defined, permittivity increases steeply (Wang and Schmugge 1980).

Wet soil is a mixture of soil particles and pore fluid. According to the Maxwell–Wagner model, the complex permittivity of such a system presents a relaxation spectrum defined by the following equation (von Hippel 1954):

$$[10] \quad \kappa^* = \kappa'_\infty + \frac{\kappa'_s - \kappa'_\infty}{1 + j\omega\tau} - j\frac{\sigma}{\omega\varepsilon_o}$$

where κ'_s is the real permittivity at low frequency, κ'_∞ is the real permittivity at frequencies beyond relaxation, σ is the conductivity of the mixture, τ is the relaxation time, and ω is the angular frequency. Double layer polarization models can be seen as generalization of this equation. The increase in concentration decreases the polarizability of the mixture (κ'_s decreases), reduces polarization losses (2nd term), but increases DC losses (3rd term). Ohmic losses prevail at low frequencies and in the case of clays with high surface charge (e.g., bentonite). At high frequencies, the effect of the conductivity term decreases, as shown in eq. 10.

Mechanical waves and geomedia (stresses)

Shear wave velocity is determined by the state of stress in particulate media, other factors such as particle geometry, void ratio, and packing being constant. Several experimental studies have been conducted to analyze the effect of the state of stress on shear wave propagation (Schultheiss 1981). Roesler (1979) showed that shear wave velocity is controlled by effective stresses in the direction of propagation and in the direction of polarization. A power equation was suggested to relate shear wave velocity to the longitudinal and the transverse effective stresses σ_l and σ_t (Roesler 1979):

$$[11] \quad V_s = \xi\left(\frac{\sigma_l}{p_a}\right)^{\chi_l}\left(\frac{\sigma_t}{p_a}\right)^{\chi_t}$$

where p_a is the normalizing atmospheric pressure, and ξ, χ_l, and χ_t are constants. If $\sigma_l = \sigma_t = \sigma_{iso}$, the previous equation reduces to

$$[12] \quad V_s = \xi\left(\frac{\sigma_{iso}}{p_a}\right)^{\gamma}$$

where the exponent γ is equal to $\gamma = \chi_l + \chi_t$. The theoretical value γ for in the case of spherical particles follows from Hertz's theory and is equal to 1/6. In the case of cone-to-plane contacts γ = 1/4. Measurements with real coarse-grained, particular materials show that γ varies from 0.16 to 0.48 (Aloufi and Santamarina 1995). The exponent γ is obtained from two or more measurements at different state of stress in devices such as isotropic, oedometric, axisymmetric, and true triaxials. Even though waves do not alter the micro-state, the change in stress does. Hence, γ not only characterizes changes in contact stiffness but also changes in microfabric (Aloufi and Santamarina 1995). The role of true effective stress (eq. 4) on shear wave propagation has not yet been assessed. Results from the experimental study reported herein will elucidate its relevance.

Experimental study: materials and devices

The experimental study was designed to monitor and to study concentration diffusion through changes in dielectric

Fig. 1. Schematic diagram of testing devices: (*A*) modified oedometer cell, and (*B*) isotropic cell.

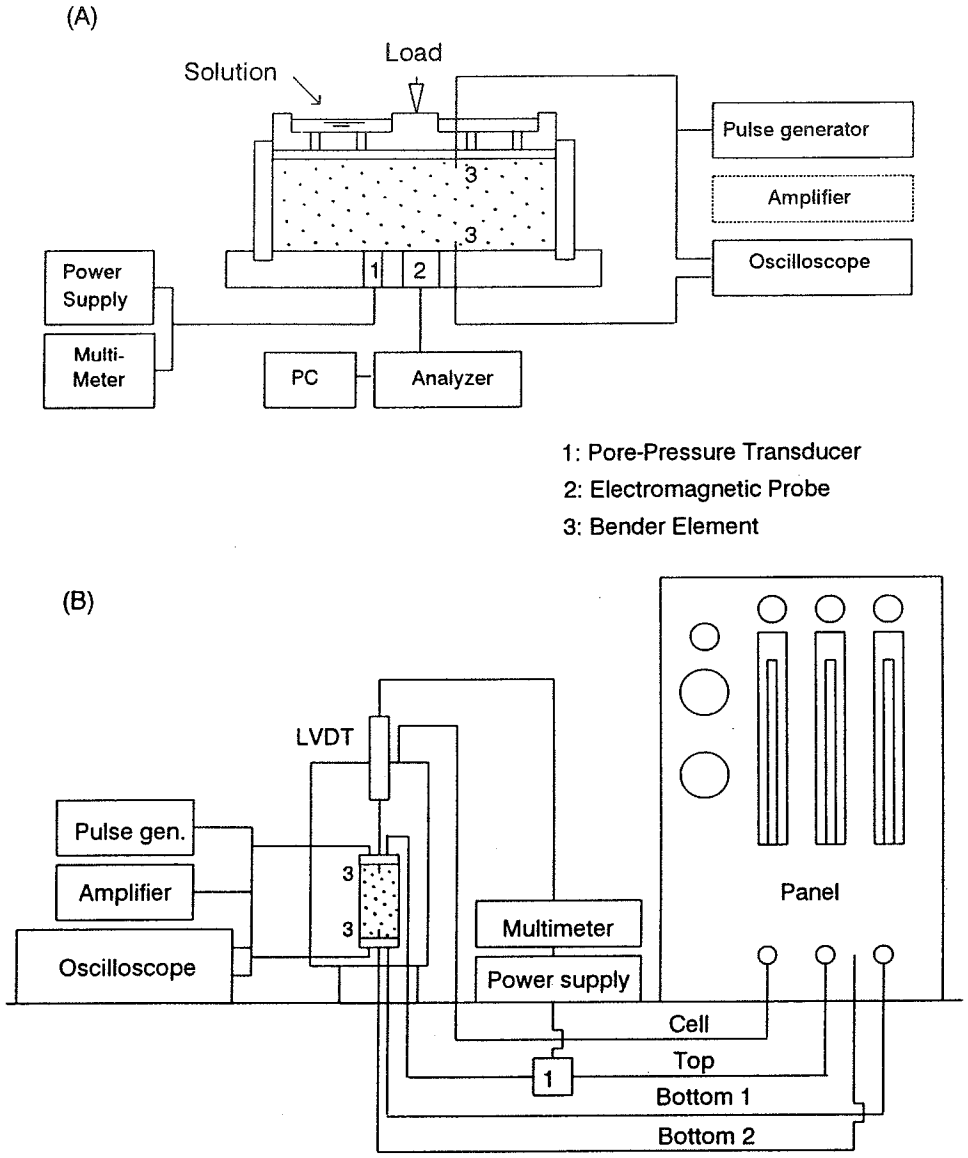

permittivity and shear wave velocity. Two testing programs were performed: the first one was conducted in a modified oedometer and the second one was performed in an isotropic cell. Three soils were tested: silica flour, kaolinite, and bentonite. They were chosen to span the range of fine particles from relatively coarse-grained, nonplastic soil (silica flour) to very fine, colloidal, plastic soil (bentonite clay). This range of particle sizes should permit assessing the effect of different interparticle forces. Physical and chemical properties of the tested soils are summarized in Table 3.

Sample preparation

Specimens were prepared using the slurry consolidation technique. Dry soil was placed in a mixer and distilled water was added continuously while mixing until the water content was twice the liquid limit ($w\ \% \approx 2\ LL.$). During mixing, vacuum was applied to the container to remove air pockets. The specimen was left in a closed container for 24 h to insure saturation, hydration, and homogeneity.

Specimens for the oedometer test were prepared by pouring the slurry inside a 100 mm inside diameter (ID) split mold with an internal rubber membrane. The mold was held on the base of a triaxial cell. The set was assembled and mounted under a gravity loading system; 50 kPa vertical pressure was applied to the clay through the loading cap. The clay was kept under load to achieve a homogeneously consolidated sample. After consolidation, the mold was removed and the water content was determined. Kaolinite and bentonite samples for isotropic testing were trimmed to 50 mm diameter.

Oedometer cell

A one-way drainage oedometric cell was designed and built to continuously measure pore pressure, shear wave velocity, and dielectric permittivity during diffusion. The

configuration of the cell is shown in Fig. 1A (Fam and Santamarina 1995). Dielectric permittivity was measured with a HP 85070A dielectric probe kit integrated to a HP 8752A network analyzer. The probe measures the dielectric permittivity in the frequency range between 0.20 and 1.30 GHz. Shear wave velocity through the sample was monitored using piezocrystal bender elements (PZT-5, APC). Reversed polarity of received signals confirmed shear wave propagation.

After completion of primary consolidation under the preselected pressure, a potassium chloride solution (KCl, 4.0 M) was continuously added to the top of the cell. In the case of silica flour and kaolinite, 610 kPa was the selected stress. However, in the case of bentonite, one loading increment (100 kPa) was conducted before diffusion to limit testing difficulties due to shorts, equipment drift, and calibration losses in excessively long test duration (each load increment requires approximately 2 weeks). The change in sample height, dielectric permittivity, shear wave velocity, and pore-water pressure were measured with time.

Isotropic cell

A modified axisymmetric flexible wall permeameter was used in this study to maintain constant vertical and horizontal confinement. Top and bottom platens were modified to include bender elements at their centers. All cables were coaxial and RTV marine silicon was used to insulate electrical components. A linear variable differential transformer (LVDT) placed inside the cell was used to monitor the vertical deformation of the sample. A three-channel triaxial control panel completed the test set-up. A schematic of the device is presented in Fig. 1B.

Bentonite and kaolinite samples were mounted in the isotropic cell and were consolidated to an initial effective stress σ_{iso} = 70 kPa. Cell, top, and bottom pressures were 415, 345, and 345 kPa. Given an initial degree of saturation of 95%, 345 kPa back pressure achieves approximately 99% degree of saturation. After initial consolidation, the cell pressure was increased by 35 kPa and all parameters were recorded with time (traveltime, LVDT reading, and volume change readings). After reaching equilibrium at σ_{iso} = 105 kPa, water was exchanged with the saturated KCl solution at the lower platen and allowed to diffuse under constant isotropic stress; free drainage was allowed from both top and bottom ports, maintaining a constant back pressure of 345 kPa. The concentration of KCl was maintained constant at the bottom platen by continuous replacement (two ports reach the porous stone, see Fig. 1B).

Results and observations

Oedometer tests

Strains

Figure 2 presents the strain–time relationship for the three soils during concentration diffusion (note: log–log plot). Bentonite shows the highest strain. The time–deformation curve during the last load increment was extrapolated to estimate the strain that would have occurred due to secondary consolidation during the time involved in chemical diffusion. Only 8% of the vertical strain measured after diffusion could be justified by secondary consolidation in both kaolinite and bentonite. The strain rate in silica flour is its creep rate (extrapolated from the prior load–deformation response).

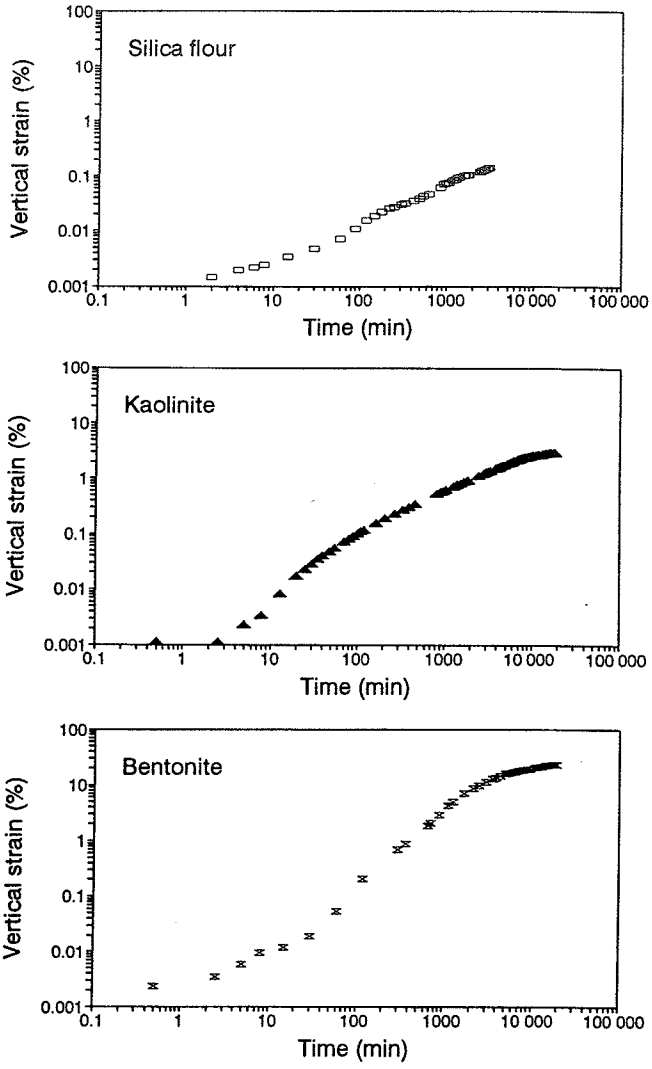

Fig. 2. Change in vertical strain with time during concentration diffusion in oedometer cell: (*A*) silica flour, (*B*) kaolinite, and (*C*) bentonite.

Pore-water pressure

A clear increase in pore pressure was observed in early stages of diffusion, followed by slow dissipation. Figure 3 presents the change in pore pressure normalized with the initial effective stress at the end of consolidation. The increase in pore pressure seems to result from the increase in true effective stresses. The unbound water (part of which may have been liberated because of the increase in concentration, eq. 5) advances in both directions ahead and backwards with respect to the concentration front. The change in pore pressure was more noticeable in bentonite where the excess pore pressure reached 40% of the initial applied effective stress; the difference in effective confinement does not permit direct comparison (100 kPa for bentonite and 610 kPa for kaolinite). In both clays, the concentration front arrived after the pore pressure started to increase.

Fig. 3. Change in pore-water pressure in oedometer cell during concentration diffusion: (*A*) bentonite, and (*B*) kaolinite samples. (The arrival time of the chemical front is estimated from the corresponding imaginary permittivity vs. time plots).

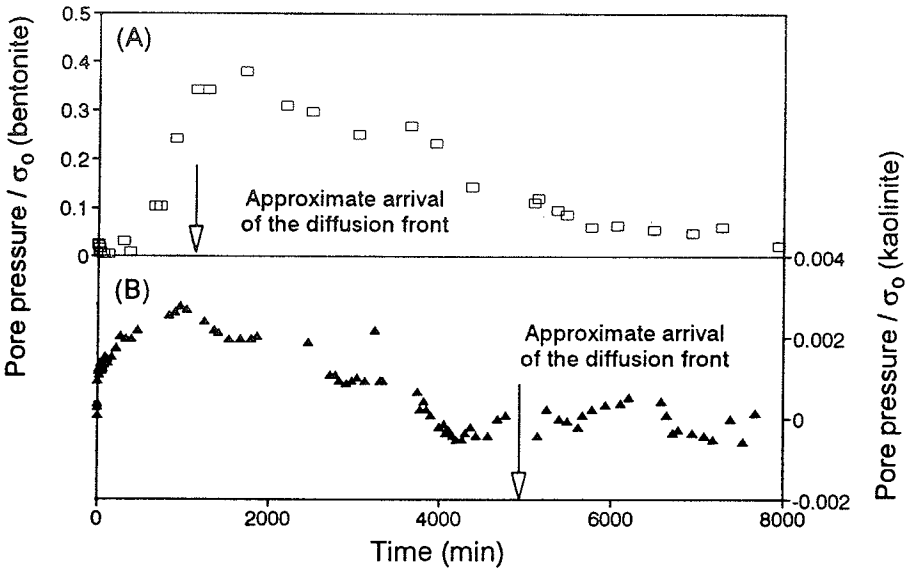

Fig. 4. Coupling phenomena during concentration diffusion. Note: Coupling equations are from Mitchell et al. (1973).

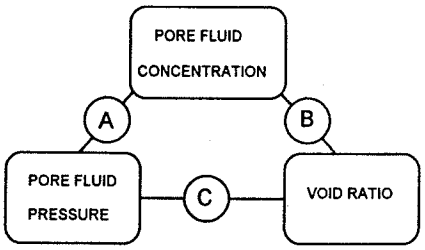

(A) Chemical-Hydraulic	(B) Chemical-Mechanical	(C) Mechanical-Hydraulic
Diffusion	Equations 14 and 15	Consolidation
$\frac{\partial c}{\partial t} = D\frac{\partial^2 c}{\partial z^2}$		$\frac{\partial u}{\partial t} = c_v\frac{\partial^2 u}{\partial z^2}$
Chemical Osmosis Coupling	Void Ratio Coupling	$\sigma' = \sigma_t - u$
$\frac{\partial u}{\partial t} = \frac{1+e}{a_v}k_{hc}\frac{\partial^2 c}{\partial z^2}$	$e\frac{\partial c}{\partial t} = -a_v c\frac{\partial u}{\partial t}$	
Drag Coupling		$\Delta\sigma' \Leftrightarrow \Delta e$
$e\frac{\partial c}{\partial t} = \frac{1+e}{\gamma_w}K_{ch}\frac{\partial}{\partial z}(x\frac{\partial u}{\partial z})$		

Fig. 5. Spectral distribution of the imaginary permittivity in oedometer cell before and after concentration diffusion: (*A*) kaolinite, and (*B*) bentonite.

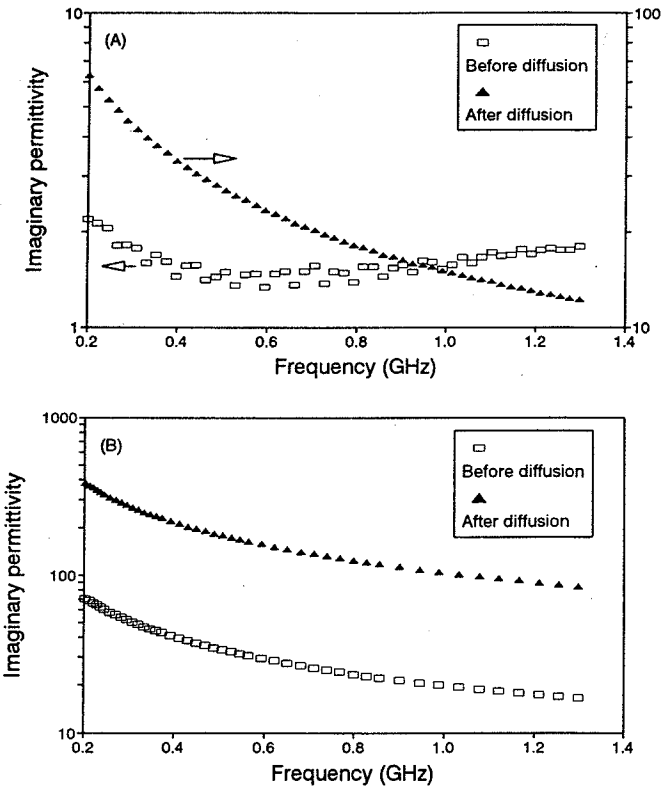

The presence of a pressure front and its early arrival are important from the point of view of monitoring and design.

Changes in void ratio, concentration, and pore pressure are coupled such that a change in one induces changes in the other two. Figure 4 is a schematic diagram of the interplay between processes and the corresponding governing equations. In the oedometer tests, there is downward diffusion of salt (concentration gradient), upward water flow

Fig. 6. Change in shear wave velocity with respect to the initial velocity during concentration diffusion in oedometer cell.

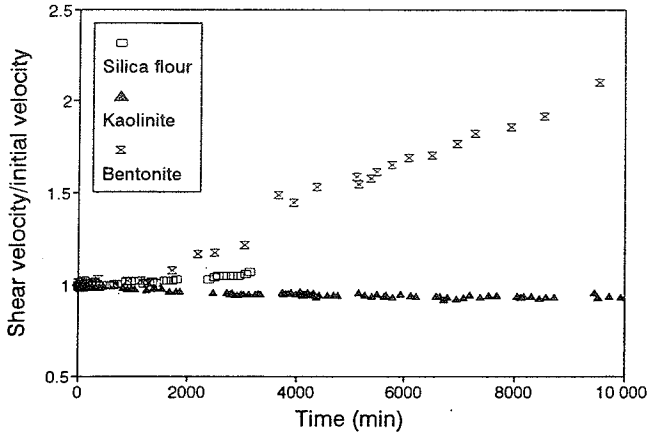

(osmotic consolidation and pressure gradient), changes in effective stress (pore-pressure changes), and changes in void ratio (true effective stress changes).

Dielectric permittivity

The complex permittivity of soils is sensitive to chemical changes in pore fluid. Spectral plots of the imaginary permittivity before and after diffusion are shown in Fig. 5. In the case of kaolinite before diffusion, the imaginary permittivity reflects the tail of the free-water relaxation ($f > 0.50$ GHz) and the beginning of double layer polarization ($f < 0.50$ GHz). However, in the case of bentonite, the tail of the free-water relaxation is masked by very high double layer polarization and a continuous increase in imaginary permittivity is observed with the decrease in frequency. After diffusion, both samples showed an increase in imaginary permittivity because of the increase in DC losses as the concentration increases and overcompensates the reduction in double layer polarization (eq. 10).

When the diffusion front reached the vicinity of the dielectric probe, the real permittivity at high frequency, 1.30 GHz, decreased slightly responding to the decrease in free-water mobility. On the contrary, the imaginary permittivity changed drastically.

Shear wave velocity

The change in shear wave velocity with time during concentration diffusion is shown in Fig. 6 where velocity values are normalized with respect to the velocity before diffusion. While no common trend can be observed among different soils, the twofold increase in velocity in bentonite is striking. Silica flour showed virtually no response to concentration changes (shear wave velocity or deformation). Note that measured traveltimes are integrals across the sample. Hence, values plotted in Fig. 6 are average velocities. Local values could be obtained through inversion procedures.

The increase in concentration produces a decrease of long-range repulsive forces, and the increase in true vertical effective stress. However, the same shrinkage mechanism can lead to lateral stress relaxation. The small decrease in

Fig. 7. Vertical strain and volume expelled from top and bottom ports for bentonite under isotropic confinement: (*A*) during consolidation from 70 to 105 kPa, and (*B*) during concentration diffusion under 105 kPa confining pressure.

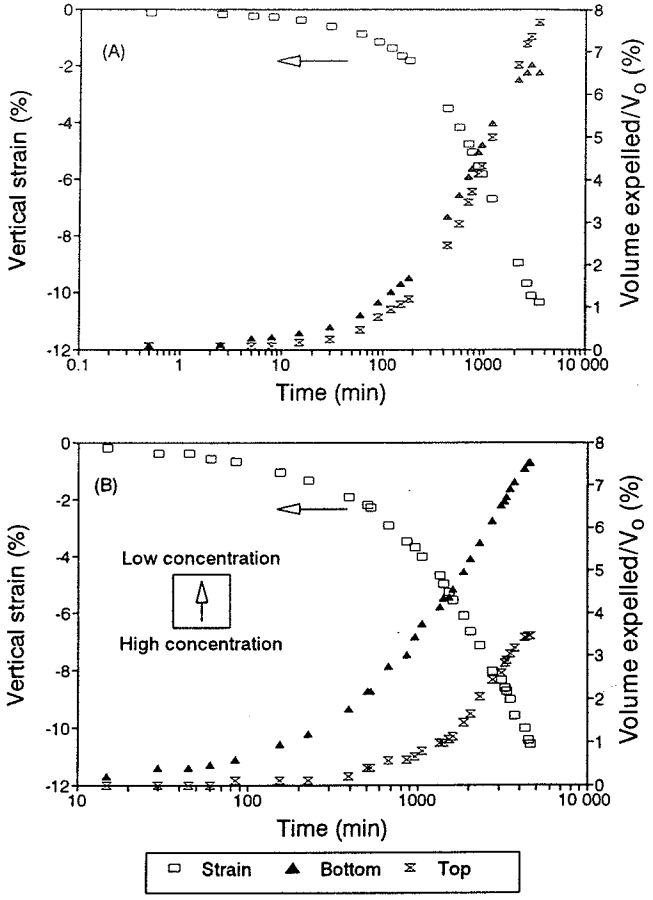

velocity in kaolinite could be explained by a prevailing effect of shrinkage and lateral stress relaxation (see eq. 11). This tentative explanation is scrutinized next by testing under isotropic confinement.

Isotropic tests

Both kaolinite and bentonite were also tested under isotropic confinement. Kaolinite and bentonite samples were 37 and 30 mm high, respectively. Pore-fluid exchange started after the end of primary consolidation, at an effective confinement σ_{iso} = 105 kPa. Measurements of axial strain, pore volume expelled, and shear wave velocity were recorded with time.

Strains

Axial strains in bentonite and the volume of expelled pore fluid during consolidation and concentration diffusion are plotted in Fig. 7. At early stages of diffusion, the volume expelled from the bottom port was larger than the volume drained from the top port (recall that fluid is exchanged at the base of the sample). After 2000 minutes, the rates of flow from both ports were almost equal. The corresponding plots for kaolinite are similar in all aspects but involve

Fig. 8. Shear wave velocity versus time before, during, and after concentration diffusion under isotropic confinement for (*A*) bentonite, and (*B*) kaolinite.

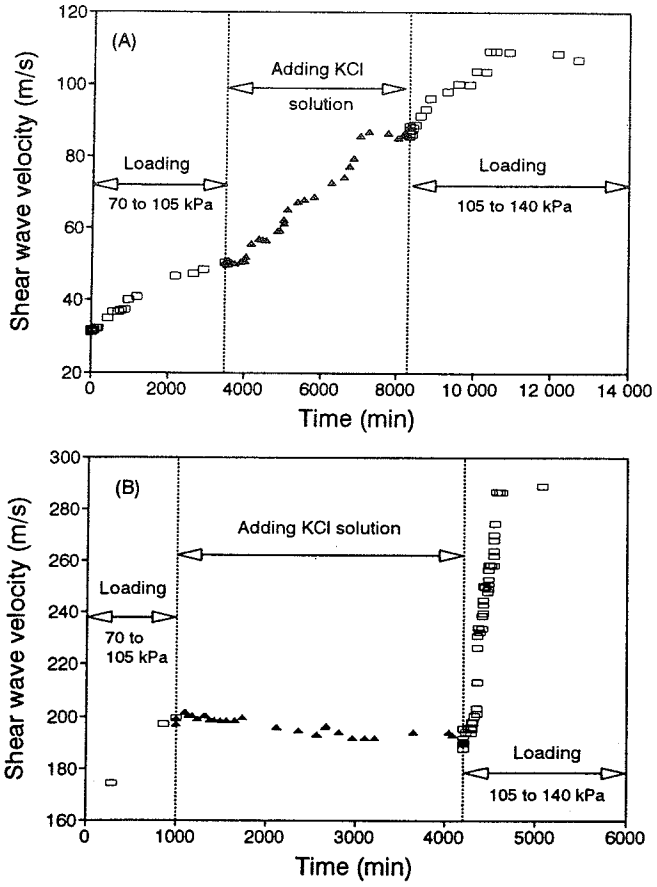

significantly lower linear and volumetric strains (ε_{vol} < 1%).

Shear wave velocity

Changes in shear wave velocity for bentonite and kaolinite are plotted in Fig. 8. Results are in agreement with the measurements in the oedometer cell. Significant increase in shear velocity (100%) was recorded in bentonite, while in kaolinite, the velocity decreased once again. An additional test was run to minimize end effects using a longer kaolinite sample d = 50 mm and H = 57 mm. Shear wave velocity showed the same result as in the shorter kaolinite sample.

Comparing results from the three kaolinite samples tested in isotropic and in oedometer cells, the earlier hypotheses of lateral stress relaxation and boundary effects are discarded. The decrease in shear wave velocity during diffusion of the high KCl concentration front appears to be the true behavior of kaolinite.

Related analyses

Strains

The decrease in sample height with the increase in porewater concentration can be explained by the change in double layer thickness and true effective stress (recall the little sensitivity of van der Waals attraction to the change in concentration). As the concentration increases, the thickness of the double layer decreases according to eq. 5, and repulsion decreases as predicted by eqs. 6 and 7. Therefore, additional settlement is expected as the concentration front advances. The smaller the particle size, the lower the skeleton force per particle, the higher the contribution of (*Rep–Att*) stress and the higher the relevance of the true effective stress concept. Testing in the isotropic cell under the same effective stress confirmed that osmotic consolidation is much more important in bentonite than in kaolinite.

Fig. 9. Theoretical change in void ratio with the change in normalized stress $P_n = \sigma_{ext}/RTc_o$ for different values of the dimensionless parameter $\Omega = \rho_w G_s A_s \vartheta$. Continuous lines correspond to mechanical consolidation at constant concentration c_o; dashed curves correspond to osmotic consolidation at constant applied stress σ_{ext}.

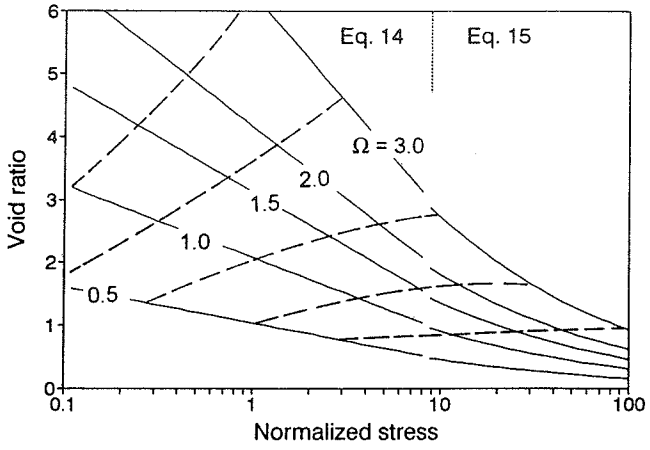

Let's consider clay particles arranged in parallel configuration. The distance between particles (d) can be related to the void ratio (e) by classical phase relations:

$$[13] \quad d = \frac{2e}{G_s A_s \rho_w}$$

where G_s is the specific gravity of the clay, A_s is the specific surface, and ρ_w is the density of water. Assuming that the repulsion pressure equals the applied stress, a relationship between void ratio, concentration, and applied stress can be derived by replacing eq. 13 into eqs. 6 and 7. In dimensionless form,

$$[14] \quad e_{LR} = \frac{\Omega}{2} \ln\left(\frac{64}{P_n}\right) \qquad d > 2\vartheta$$

$$[15] \quad e_{SR} = \frac{\pi\Omega}{\sqrt{P_n + 2}} \qquad d < 2\vartheta$$

where $\Omega = G_s A_s \rho_w \vartheta$, and $P_n = \sigma_{ext}/RTc_o$ is the normalized applied stress. These equations are plotted in Fig. 9, in an e – log P_n plot. Curves in continuous lines characterize standard mechanical consolidation due to the increase in applied stress, at constant concentration. The family of curves in dashed lines represents void ratio changes at constant applied stress when clays are subjected to increased

Fig. 10. Measured and predicted changes in the imaginary permittivity with time for silica flour during concentration diffusion in oedometer cell (the inverted apparent diffusion coefficient is 9×10^{-10} m^2/s).

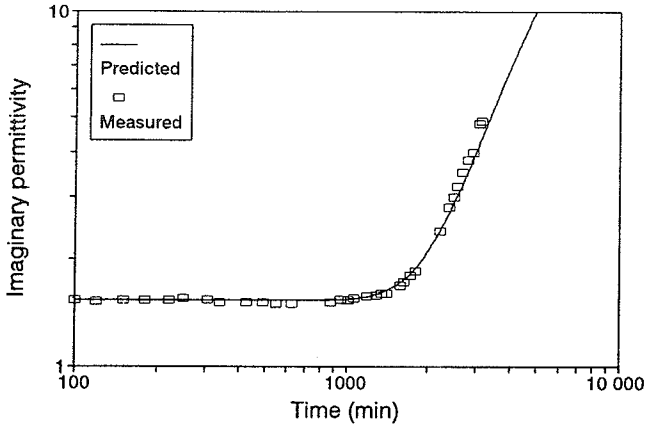

Fig. 11. Measured and predicted distributions of the imaginary permittivity in the silica flour sample at the end of concentration diffusion in the oedometer cell (the inverted apparent diffusion coefficient is 9×10^{-10} m^2/s).

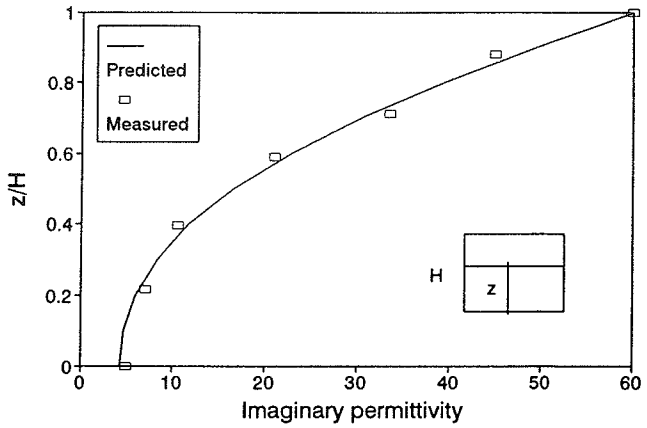

concentration during osmotic consolidation. It can be seen that the higher the applied stress, the smaller the osmotic consolidation.

The value of these equations is qualitative. Deviations from actual measurements are in part due to parallel particle assumption. According to Meade (1964), the parallel particle condition may be valid at high stresses, as the degree of preferred orientation increases with the applied stress. Mitchell (1993) indicates that this type of analysis loses validity for clays with particle dimension more than 0.20 μm. Comparison of experimental and theoretical results shows that the higher the concentration, the larger the deviation from the experimental curve, probably because other interparticle forces gain relevance at close distances.

Dielectric permittivity

A linear relationship between concentration of water solutions and imaginary permittivity was observed in calibration tests (the correlation coefficient $r = 0.997$),

$$[16] \quad \kappa'' = a + bc$$

Substituting this relationship into Fick's second law (eq. 2), the following expression is obtained:

$$[17] \quad \frac{\partial \kappa''}{\partial t} = D\frac{\partial^2 \kappa''}{\partial z^2}$$

or, in finite difference form,

$$[18] \quad \kappa''_{i,j+1} = \frac{\Delta t D}{\Delta z^2}(\kappa''_{i+1,j} - 2\kappa''_{i,j} + \kappa''_{i-1,j}) + \kappa''_{i,j}$$

where i is the subscript for node position, and j is for node time; Δt is the time interval and Δz is the depth interval between nodes; and D is the apparent diffusion coefficient. The above equation can be written in matrix form as:

$$[19] \quad [\boldsymbol{\kappa}'']_m = [\boldsymbol{M}]^m [\boldsymbol{\kappa}''_0]$$

where $[\boldsymbol{\kappa}'']_m$ is the vector of imaginary permittivity after m time intervals, $[\boldsymbol{M}]$ is the matrix of coefficients, and $[\boldsymbol{\kappa}''_0]$ is the initial vector of imaginary permittivity at time zero.

Measured trends of imaginary permittivity versus time were used to invert for the apparent diffusion coefficient for the three soils, using eq. 19 and appropriate boundary conditions. Inversion was driven to minimize the sum of the square error between predicted and measured imaginary permittivity values. It was observed that the error function is very sensitive to the selected diffusion coefficient. Figure 10 shows the predicted and measured changes in imaginary permittivity with time in the case of silica flour. The fit is excellent for the three soils. Applying this technique, the inverted apparent diffusion coefficients were: 9×10^{-10}, 5×10^{-10}, and 3×10^{-10} m^2/s for silica flour, kaolinite and bentonite, respectively.

The apparent diffusion coefficient can also be obtained at the end of the test by slicing the specimen and measuring the imaginary permittivity at different heights. Equation 19 can then be fitted to the measured values to determine the diffusion coefficient. Figure 11 shows the predicted distribution of imaginary permittivity computed with the apparent diffusion coefficient inverted from permittivity–time data and the measured values (Figs. 10 and 11 are similar for the three soils).

Shear wave velocity

While the compiled experimental evidence discussed earlier may elucidate apparent contradictory data found in the literature, the changes in kaolinite upon the increase in concentration remain unaccounted. Hypotheses must explain the decrease in shear wave velocity and the concurrent increase in density (when changes in velocity and density are taken into consideration, the computed change in shear modulus shows a decrease in stiffness between 10 and 20%; $G = \rho V_s^2$). While shrinkage is due to the reduction in repulsion forces and the increase in true effective stress, the decrease in stiffness must reflect the effect of another process that overcomes the normally stiffening effect associated with increased stresses.

This additional process may include the development of a less-rigid fabric because of the loss of edge-to-face contacts, the change in short-range hydration forces, the change in edge-charges. Detailed analyses of these mechanisms

are cumbersome. Consider for example short-range hydration forces: molecules between two surfaces tend to adopt positions that lead to minimum total energy. As particles move closer together, minimum energy conditions are altered generating a force that oscillates with distance. This force may be preferentially attractive or repulsive depending on a variety of surface and fluid properties and may affect a range of 1 to 3 nm (Horn et al. 1989; Israelachvili 1991). These hypotheses do not imply that kaolinite becomes "weaker" after concentration diffusion: strength is a large strain parameter that induces massive fabric changes.

Finally, it is important to note that montmorillonite particles are lattice expansive colloids with very significant long-range double layer effects; however, kaolinites are larger particles (in the transition to noncolloidal) and carry a much higher skeleton force per particle than bentonites. McConnachie (1974) showed that short-range forces prevail in kaolinite when the effective confinement exceeds 15 kPa. Fabric changes due to osmotic effects become increasingly more restricted with the increase in interparticle forces.

Conclusions

The effect of concentration diffusion on clay behavior was investigated with mechanical and electromagnetic waves. Results show a variety of unique phenomena and give new insight into the complex nature of clay behavior.

The behavior of clays can be adequately explained in most cases by considering long-range double layer repulsion and van der Waals attraction. The larger the particles and the higher the applied stress, the higher the force-per-particle. Eventually, interparticle spacing may become small enough to activate short-range hydration forces.

The concentration front is preceded by a pressure front that results from the coupling between pressure and concentration gradients, changes in double layer, liberation of adsorbed water, increase in true effective stress, and associated changes in fabric. The pressure front is very significant in soft bentonite.

The complex permittivity of soils reflects changes in double layer. Changes in imaginary permittivity with time during concentration diffusion can be used to estimate the "apparent diffusion coefficient."

The propagation of stress waves is determined by interparticle forces. In coarse granular materials, Newtonian forces are significant and the velocity of propagation is related to Terzaghi's state of effective stress. In fine materials, electrical forces must be included. These may play a dual role, either increasing or decreasing velocity: in the case of bentonite, the effect is through long-range forces, however, kaolinite seems to be affected also by oscillatory short-range hydration forces. In addition, changes in edge-charges and the development of denser, yet less-stiff fabrics may add to the observed behavior. Detailed interpretation of these phenomena is cumbersome.

Acknowledgments

This study is part of a research project on wave–geomedia interaction and applications. Funding is provided by the Natural Sciences and Engineering Research Council of Canada (NSERC). Hewlett Packard support and valuable comments by E. Reardon, M. Geilikman, and the reviewers are gratefully acknowledged.

References

Aloufi, M., and Santamarina, J.C., 1995. Low and high strain macrobehavior of grain masses—the effect of particle eccentricity. American Society of Agricultural Engineering, ASAE Publication, **38**(3): 877–887.

Barbour, S.L., and Yang, N. 1993. A review of the influence of clay–brine interactions on the geotechnical properties of Ca-montmorillonitic clayey soils from western Canada. Canadian Geotechnical Journal, **30**: 920–934.

Bolt, G.H. 1956. Physico-chemical analysis of the compressibility of pure clays. Géotechnique, **6**(2): 86–93.

Bowders, J.J. 1985. The influence of various concentrations of organic liquids on the hydraulic conductivity of compacted clay. The University of Texas at Austin, Geotechnical Engineering Dissertation GT85-2.

DiMaio, C., and Fenelli, G.B. 1994. Residual strength of kaolin and bentonite: the influence of their constituent pore fluid. Géotechnique, **44**(4): 217–226.

Dunn, R.J., and Mitchell, J.K. 1984. Fluid conductivity testing of fine grained soils. Journal of Geotechnical Engineering, ASCE, **110**(GT11): 1648–1665.

Everett, D.H. 1988. Basic principles of colloid science. The Royal Society of Chemistry, Picadilly, London.

Fam, M., and Santamarina, J.C. 1995. Study of geoprocesses with complementary mechanical and electromagnetic wave measurements in an oedometer. Geotechnical Testing Journal, ASTM, **18**(3).

Fritz, S.J., and Marine, I.W. 1983. Experimental support for a predictive osmotic model of clay membranes. Geochimica et Cosmochimica Acta, **47**: 1515–1522.

Hasted, J.B. 1973. Aqueous dielectrics. Chapman & Hall, London.

Horn, R.G., Smith, D.T., and Haller, W. 1989. Surface forces and viscosity of water measured between silica sheets. Chemical Physics Letters. **162**: 404–408.

Israelachvili, J. 1991. Intermolecular and surface forces. Academic Press, London.

Kenney, T.C. 1967. The influence of mineral composition on the residual strength of natural soils. Proceedings of the Geotechnical Engineering Conference, Oslo, Vol. 1, pp. 123–129.

Lyklema, J. 1991. Fundamentals of interface and colloid science. Volume 1: fundamentals. Academic Press, London.

Madsen, F.T., and Mitchell, J.K. 1989. Chemical effects on clay hydraulic conductivity and their determination. Mitteilungen des Institutes fur Grundbau und Bodenmechanik Eidenossische Technische Hochschule, Zurich, Report No. 135.

McConnachie, I. 1974. Fabric change in consolidated kaolin. Géotechnique, **24**(2): 207–222.

Meade, R. 1964. Removal of water and rearrangement of particles during the compaction of clayey sediments—review. Geological Survey, Professional Paper 479-B, U.S. Government Printing Office, Washington, pp. 1–23.

Mesri, G., and Olsen, R.E. 1970. Shear strength of montmorillonite. Géotechnique, **20**(3): 261–270.

Mesri, G., and Olsen, R.E. 1971. Consolidation characteristics of montmorillonite. Géotechnique, **21**(4): 341–352.

Mitchell, J.K. 1991. Conduction phenomena: from theory to geotechnical practice. Géotechnique, **41**(3): 299–340.

Mitchell, J. K. 1993. Fundamentals of soil behavior. 2nd ed. John Wiley & Sons Inc., New York.

Mitchell, J.K., Greenberg, J.A., and Witherspoon, P.A. 1973.

Chemico-osmosis effects in fine-grained soils. Journal of Soil Mechanics and Foundation Division, ASCE, **99**(SM4): 307–321.

Moore, C.A. and Mitchell, J.K., 1974. Electromagnetic forces and soil strength. Géotechnique, **24**(4): 627–640.

Moore, R. 1991. The chemical and mineralogical controls upon the residual strength of pure and natural clays. Géotechnique, **41**(1): 35–47.

Morgenstern, N.R. 1969. Structural and physico-chemical effects on the properties of clays. Proceedings of the 7th International Conference on Soil Mechanics and Foundation, Mexico, Vol. 3, pp. 455–471.

Quirk, J.P., and Schofield, R.K. 1955. The effect of electrolyte concentration on soil permeability. Journal of Soil Science, **6**(2): 163–178.

Roesler, S.K. 1979. Anisotropic shear modulus due to stress anisotropy. Journal of the Geotechnical Engineering Division, ASCE, **105**(GT7): 871–880.

Rowe, R.K., Caers, C.J., and Barone, F. 1988. Laboratory determination of diffusion and distribution coefficients of contaminants using undisturbed clayey soil. Canadian Geotechnical Journal, **25**: 108–118.

Schultheiss, P.J. 1981. Simultaneous measurements of P & S wave velocities during conventional laboratory soil testing procedures. Marine Geotechnology, **4**(4): 343–367.

Shachelford, D.C., and Daniel, D.E. 1991. Diffusion in saturated soils: I: Background. Journal of Geotechnical Engineering, ASCE, **117**(3): 467–484.

Shang, J. Q., Lo, K.Y., and Quigley, R.M. 1994. Quantitative determination of potential distribution in Stern-Gouy double-layer model. Canadian Geotechnical Journal, **31**: 624–636.

Sivapullaiah, P.V., and Sridharan, A. 1987. Effect of polluted water on the physico-chemical properties of clayey soils. *In* Environmental geotechnics and problematic soils and rocks. *Edited by* Balasubramaniam, S. Chandra, D.T. Bergado, and P. Nutalaya. Balkema, Rotterdam, pp. 179–190.

Sridharan, A., and Rao, V.G. 1973. Mechanisms controlling volume change of saturated clays and the role of effective stress concept. Géotechnique, **23**(3): 359–382.

Sridharan, A., and Rao, V.G. 1979. Shear strength behavior of saturated clays and the role of effective stress concept. Géotechnique, **29**(2): 177–193.

Sridharan, A., and Sivapullaiah, P.V. 1987. Engineering behavior of soils contaminated with different pollutants. *In* Environmental geotechnics and problematic soils and rocks. *Edited by* Balasubramaniam, S. Chandra, D.T. Bergado, and P. Nutalaya. Balkema, Rotterdam, pp. 165–178.

van Olphen, H. 1977. An introduction to clay colloid chemistry. 2nd ed. John Wiley & Sons, New York.

von Hippel, A.R. 1954. Dielectric and waves. 1st student ed. John Wiley & Sons, Inc., New York.

Wang, J.R., and Schmugge, T.J. 1980. An empirical model for the complex dielectric permittivity of soil as a function of water content. IEEE Transactions on Geoscience and Remote Sensing, **GE-18**: 288–295.

Warkentin, B.P. 1961. Interpretation of the upper plastic limit of clays. Nature (London), **190**: 287–288.

Yong, R.N., and Warkentin, B.P. 1975. Soil properties and behavior. Geotechnical Engineering 5, Elsevier Scientific Publication Co., New York.

List of symbols

η	viscosity, $kg \cdot s^{-1} \cdot m^{-1}$
ω	angular frequency, $rad \cdot s^{-1}$
τ	relaxation time, s
σ	conductivity, $S \cdot m^{-1}$
ψ_o	surface potential, V
Ω	dimensionless parameter = $G_s A_s \rho_w \vartheta$
ρ	density, kgm^{-3}
ϑ	double layer thickness, m
ϕ	angle of shearing resistance
σ'	effective stress, Pa
κ'	relative real dielectric permittivity
κ'_∞	optical dielectric permittivity
κ''	relative imaginary dielectric permittivity
κ'_s	static dielectric permittivity
κ^*	complex dielectric permittivity
σ_{ext}	external applied stress, Pa
σ_{iso}	isotropic stress, Pa
σ_l	stress in the longitudinal direction, Pa
σ_m	true effective stress, Pa
σ_t	stress in the transverse direction, Pa
σ_{tot}	total stress, Pa
A	Hamaker constant, Pa·m
a	radius of the chemical species, m
A_s	specific surface, $m^2 \cdot kg^{-1}$
Att	attractive stress between clay particles, Pa
c	concentration, $mol \cdot m^{-3}$
C^*	shear intercept, Pa
c_o	ion concentration in the bulk solution, $mol \cdot m^{-3}$
D	apparent diffusion coefficient, $m \cdot s^{-2}$
d	spacing between particles, m
D_o	diffusion coefficient of certain species, $m^2 \cdot s^{-1}$
E	electrical field, $V \cdot m^{-1}$
e	void ratio
ε_o	permittivity of vacuum, $8.854 \cdot 10^{-12}$ $C^2 \cdot J^{-1} \cdot m^{-1}$
F	Faraday's constant, $9.6487 \cdot 10^4$ C/mol
G_s	specific gravity of solids
H	sample height, m
J	mass flux, $mol \cdot s^{-1} \cdot m^{-2}$
k	Boltzmann's constant, $1.38 \cdot 10^{-23}$ $m^3 \cdot Pa \cdot K^{-1}$
k_p	hydraulic conductivity, $m \cdot s^{-1}$
LL	liquid limit
P	polarization field, $C \cdot m^{-2}$
p_a	atmospheric pressure, Pa
P_n	normalized stress = σ_{ext}/RTc_o
R	universal gas constant, 8.314 $m^3 Pa \cdot mol^{-1} \cdot K^{-1}$
Rep	repulsive stress between clay particles, Pa
T	temperature, K
t	time, s
u_o	pore water pressure, Pa
v	valence of ion species
V_s	secondary wave velocity (shear wave velocity), $m \cdot s^{-1}$
w	water content
z	distance, m